Materials Science and Engineering A 410–411 (2005) 364–368

www.elsevier.com/locate/msea

Characteristics of aluminum 6061-T6 deformed to large plastic strains by machining

M. Ravi Shankar [a], Srinivasan Chandrasekar [a,*], W. Dale Compton [a], Alexander H. King [b]

[a] *School of Industrial Engineering, Purdue University, West Lafayette, IN 47907, USA*
[b] *School of Materials Engineering, Purdue University, West Lafayette, IN 47907, USA*

Received in revised form 1 March 2005

Abstract

A study has been made of characteristics of precipitation treatable aluminum alloys (6061-T6) deformed to large plastic strains, by analyzing chips created by plane strain (2-D) machining. By varying the geometry of the tool, different levels of strain were imposed in the chip in a single pass of machining. The microstructure of the chips was found to be composed of relatively equi-axed grains with mean size in the range of 70–100 nm. The evolution of the microstructure across the deformation zone has been tracked. The chip micro-hardness values were found to be somewhat greater than that reported for Al 6061-T6 deformed by equal channel angular pressing (ECAP).

Keywords: SPD; Aluminum; 6061; Machining; Ultra-fine; Nanostructure

1. Introduction

Precipitation treatable aluminum alloys, e.g. Al 6061-T6, are some of the most promising candidates for fabricating thermally stable, high-strength and light-weight nanostructured materials through large strain deformation. The presence of the precipitate phase is expected to impart thermal stability to the nanostructured metallic matrix in addition to enhancing strength. Most of the research into the characteristics of highly deformed, precipitation treatable aluminum alloys has relied on the use of severe plastic deformation (SPD) methods such as equal channel angular pressing/extrusion (ECAP/ECAE) to impose the large strains [1–6]. In addition to demonstrating the formation of nanocrystalline microstructures, these studies have shown that the presence of second phase particles indeed imparts thermal stability to the ultrafine grained microstructure produced by SPD [1,6]. Recently, some evidence has been found suggesting an acceleration of grain refinement during SPD that is brought about by the presence of the second phase particles/precipitates [7].

Precipitation-treatable alloys, when peak aged (T6 temper), have an optimum distribution of precipitates that ensures the greatest strength for the material. Thus, large strain deformation of aluminum alloys in the T6 temper offers a vehicle for the production of nanostructured materials that have a fine dispersion of precipitates distributed uniformly throughout the matrix. However, the considerable strength of these alloys in the T6 temper offers a challenge to subjecting these alloys to SPD at room temperature. This is probably the reason why nearly all of the ECAE research on these alloys to date has been performed at elevated temperatures or in the overaged/solution treated condition.

Due to the simplicity of the plane strain (2-D) machining process, it is possible to deform peak aged aluminum alloys to large values of shear strain even at room temperature. Thus, it is our preferred method for introducing very large strains. Furthermore, with a suitable choice of the tool rake angle (α), it is possible to impose shear strains of 1–10 in the chip.

1.1. Machining

Fig. 1 shows a schematic of a plane strain (2-D) machining process and associated geometric parameters. The amount of interference between the tool and the bulk, viz. the undeformed chip thickness (a_o), the relative velocity between the tool and the bulk (V_o) and the tool rake angle (α) are the principal machining parameters. When the tool cutting edge is perpendicular to the cutting velocity and the width of cut is large compared to a_o, a state of plane strain deformation prevails during chip formation. Chip formation occurs by concentrated shear (large

* Corresponding author. Tel.: +1 765 494 3223; fax: +1 765 494 5448.
E-mail address: chandy@ecn.purdue.edu (S. Chandrasekar).

0921-5093/$ – see front matter © 2005 Elsevier B.V. All rights reserved.
doi:10.1016/j.msea.2005.08.137

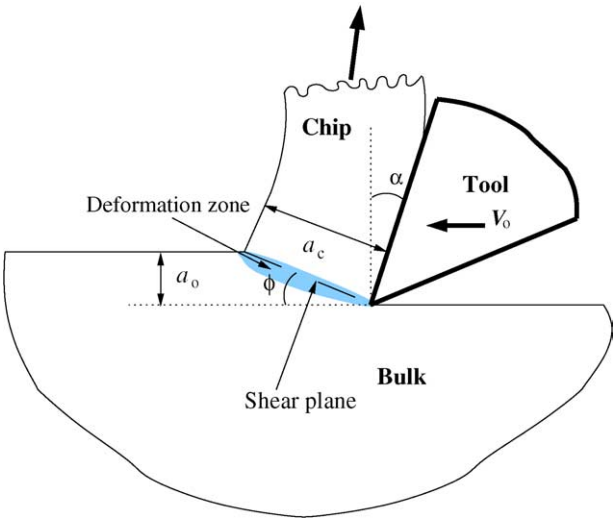

Fig. 1. Schematic of plane strain (2-D) machining.

strain deformation) in a small, distinct deformation zone, often idealized as a shear plane. The geometry of this deformation zone is completely determined by the shear plane angle (ϕ) and the rake angle (α). The uniform shear strain (γ) imposed during deformation is given by [8]:

$$\gamma = \frac{\cos\alpha}{\sin\phi\cos(\phi-\alpha)} \quad (1)$$

where ϕ is calculated from a measurement of a_o and a_c (Fig. 1), as:

$$\tan\phi = \frac{(a_o/a_c)\cos\alpha}{1-(a_o/a_c)\sin\alpha} \quad (2)$$

2. Experimental procedure

Chips were produced by plane strain machining of 2 mm wide Al 6061-T6 sheet with high speed steel tools of rake angle $+5^\circ$ and -20°. The undeformed chip thickness (a_o) was set at 100 μm and the chip width was ∽ 2 mm. A sufficiently low velocity of 10 mm/s was employed to ensure minimal temperature rise during chip formation. The grain size of the Al6061-T6 bulk was ∽ 75 μm and its Vickers hardness was 110 kg/mm^2.

Partially detached chip specimens such as those shown in Fig. 2 were created in a specially devised "quick stop" experiment to examine the microstructure changes occuring in the deformation zone. Optical metallography of these specimens showed the bulk material to be composed of relatively large equi-axed grains (∽ 75 μm) while the chips exhibited a "flow-line" type microstructure characteristic of material deformed to large plastic strains; these features can be seen in Fig. 2.

The microstructure of the chips was studied using transmission electron microscopy (TEM). Under plane strain machining conditions, the chips tended to curl considerably. Furthermore, the chips produced with the negative rake angle tools often fragmented (Fig. 2(b)). Hence, wedge polishing followed by ion milling was used, rather than electrolytic thinning, to produce the TEM specimens. Care was taken to avoid any prolonged heating of the specimens during the mechanical thinning and ion milling in order to ensure the integrity of the microstructure of the as-machined chip.

In the wedge polishing, the specimens were first mechanically thinned by abrasive polishing to form shallow wedges. Each wedge was then mounted on a copper slot grid and ion milled for a very short duration of time (∽ 5–10 min) in a Gatan Model 600 Dual Ion Mill to create an electron transparent specimen.

To track the evolution of microstructure in the deformation zone with the TEM, some of the partially detached chip specimens were first mechanically thinned to about 200 μm in thickness. Then an area of interest was cut out and mechanically thinned to form a shallow wedge, as shown in an exaggerated manner in Fig. 3. Following mechanical thinning, each wedge was mounted on to a copper slot grid and ion milled for about 15 min at room temperature in a Model 600, Gatan Dual Ion Mill.

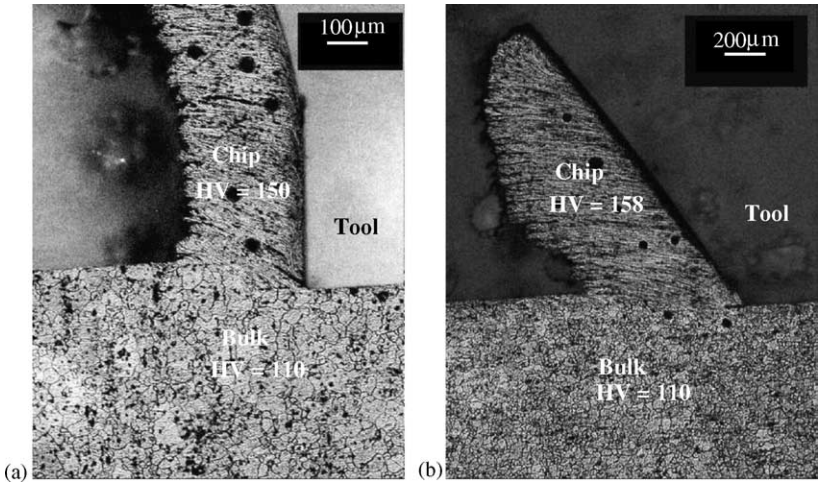

Fig. 2. Optical micrographs of partially detached chip specimens produced with (a) $+5^\circ$ rake angle tool and (b) -20° rake angle tool. The specimens have been polished and etched to develop the microstructure. Note the sharp transition from the microstructure of the bulk, characterized by grains ∽ 75 μm in size, to the "flow-line" type microstructure of the chip indicative of large strain deformation. The transition region may be identified with the large strain deformation zone.

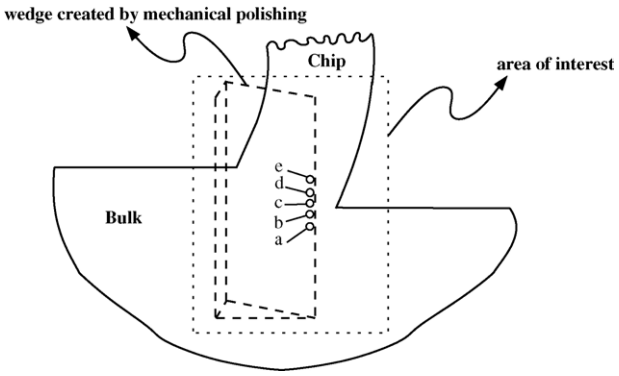

Fig. 3. Technique used to study microstructure evolution across the shear plane. The letters a,b,c,d,e refer to the locations from which the images in Fig. 6 are obtained.

The electron transparent specimens were examined in a JEOL 2000FX Transmission Electron Microscope operated at an accelarating voltage of 200 kV.

3. Results and discussion

3.1. Hardness and grain size

The shear strain in the chip, as estimated using Eqs. (1) and (2), generally increases with decreasing rake angle. This shear strain was $\backsim 3.2$ in the chip machined with a $+5^\circ$ rake angle tool and $\backsim 5.2$ in the chip machined with a -20° rake angle tool. We note in Fig. 2 that for the same value of the undeformed chip thickness (a_o), the thickness of the chip (a_c) machined with the -20° rake tool is significantly larger than that for the $+5^\circ$ rake chip. Consequently, the shear angle (ϕ) for the -20° rake chip is much smaller than the shear angle for the $+5^\circ$ rake angle chip and thus, the shear strain imposed during chip formation with the -20° rake tool is larger. The Vickers hardness values for the $+5^\circ$ and -20° rake angle chips were found to be 150 ± 3HV and 158 ± 3HV, respectively. Not only is this difference statistically significant, but also both of these hardness values are significantly greater than that measured ($\backsim$ 130HV) on Al 6061-T6 produced by warm ECAP [1], indicating a strong effect of deformation temperature.

TEM study of the chips produced with the $+5^\circ$ and -20° rake angle tools revealed a very fine microstructure and a diffraction pattern characteristic of a random orientation of subgrains, as shown in Figs. 4 and 5. The typical grain size in the chips was less than 100 nm. In the chips resulting from machining with a $+5^\circ$ rake angle tool ($\gamma = 3.2$), the grain size was 82 ± 30 nm while in the -20° rake angle chips ($\gamma = 5.2$) the grain size was 75 ± 20 nm. The average grain size in the bulk was found to be 75 μm, by optical metallography.

3.2. Cell misorientation angles

Convergent beam electron diffraction (CBED) was used to identify the orientations of the constituent grains/cells in the chips and, subsequently, to calculate the misorientation angles.

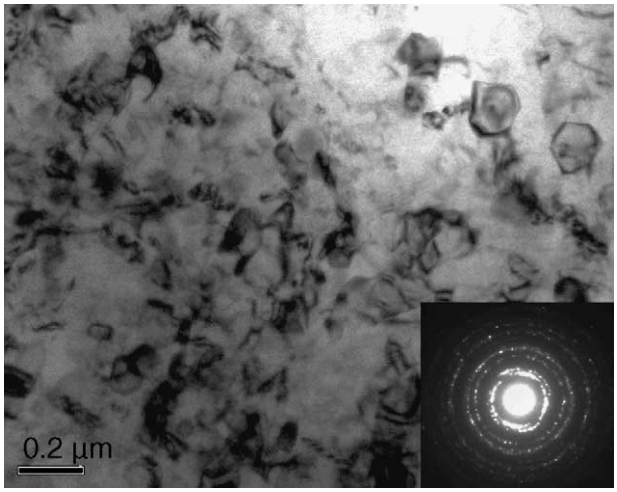

Fig. 4. Bright field TEM image of chips produced with the $+5^\circ$ rake angle tool ($\gamma = 3.2$). The average grain size in the chips is 82 nm and the hardness is 150 HV.

For this purpose, the CBED patterns were first identified and indexed. Then, the orientation matrix of each grain was determined by taking into consideration the rotations required to align the crystallographic axes with conveniently chosen "room coordinates". The misorientation angles and axes were then extracted from these orientation matrices. The average misorientations between grains in the -20° rake angle chips was found to be $\backsim 20^\circ$ (large-angle boundaries) while that for the $+5^\circ$ rake angle chips was $\backsim 10^\circ$ (medium-angle boundaries).

This observation is in line with the accepted notion of a monotonic increase in misorientation angles with increasing values of strain. A power-law variation of the form $\theta \backsim M_o \epsilon^{M_1}$ has been postulated to relate the the average cell-misorientation angle θ to the imposed strain ϵ [9]. Consequently, a monotonic increase is expected in the dislocation density and the associated hardness value with increasing strain. This appears to be the operative

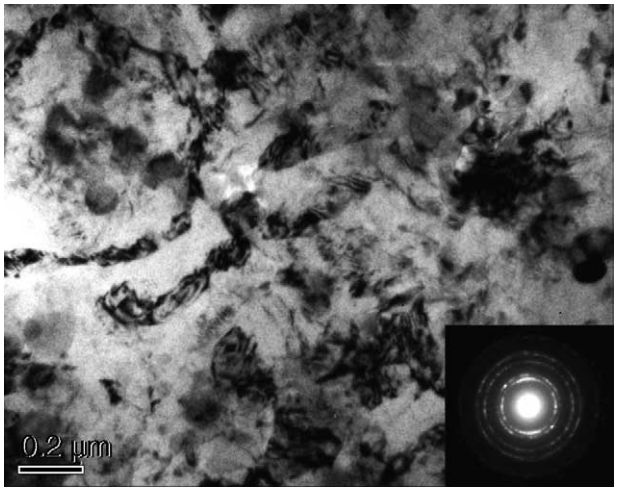

Fig. 5. Bright field TEM image of chips produced with the -20° rake angle tool ($\gamma = 5.2$). The average grain size in the chips is 75 nm and the hardness is 158 HV.

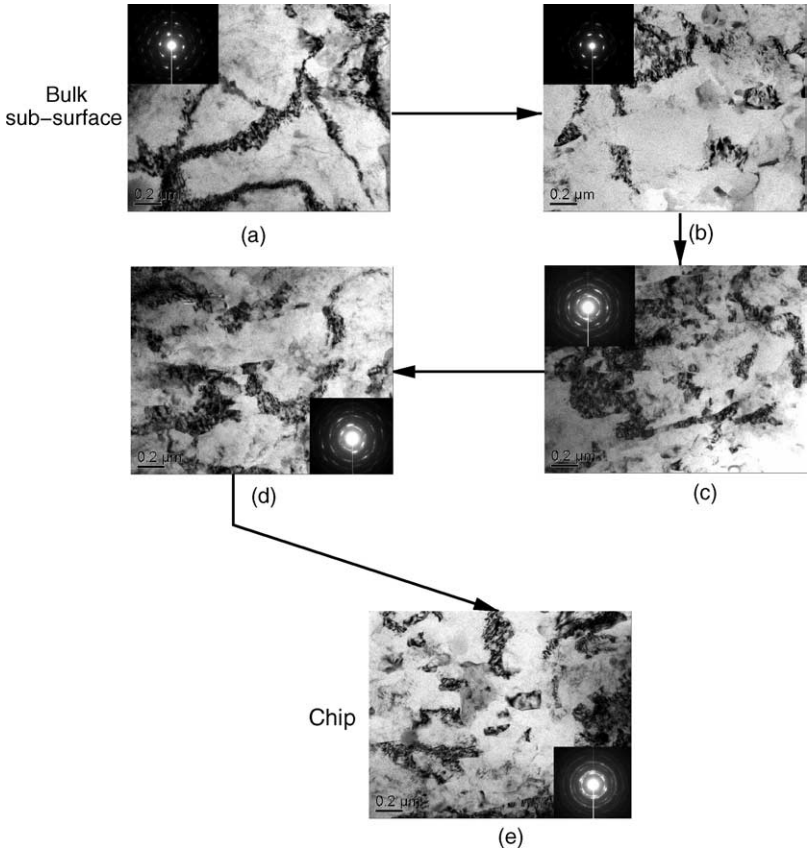

Fig. 6. TEM images of partially detached chip showing progression of microstructure across the deformation zone. (a) Rudimentary dislocation cell structures in the bulk sub-surface, (b) low misorientation angle cellular microstructure in the deformation zone closest to the bulk, (c) formation of progressively refined, highly misoriented sub-grains about mid-way through the deformation zone, (d) continued refinement of the microstructure in the deformation zone closer to the chip and (e) final microstructure of the chip.

phenomenon that might be responsible for the observed increase in hardness value with strain in the chips.

3.3. Evolution of microstructure

The thinned, partially formed chip samples were examined under the TEM to study the evolution of the microstructure across the deformation zone. Fig. 6 shows a sequence of TEM images from one such sample at different locations in and around the deformation zone, while progressing from the bulk into the chip. Dislocation activity is seen to extend far from the primary deformation zone in Fig. 6(a) indicative of substantial sub-surface damage to the bulk. The dislocation networks are mostly in the form of carpets and some rudimentary, low-misorientation angle cells that are typically larger than 1 μm in size. In moving towards the deformation zone in Fig. 6, the material appears to develop a fine cellular microstructure typically about 100–200 nm in size even at a considerable distance (typically tens of micrometers) from the deformation zone (Fig. 6(b)). A progressive refinement of the microstructure is seen in areas closer and closer to the chip, wherein, the large dislocation carpets far into the bulk appear to give way to cells that are about 200 nm in size (Fig. 6(c)); these cells in turn refine to about 100 nm in areas closer to the chip (Fig. 6(d)). The final microstructure of the chip is seen to be comprised of nano-scale, equi-axed grains as shown in Fig. 6(e).

The diffraction pattern of the cellular microstructure farthest from the deformation zone (Fig. 6(b)) indicates the presence of only very small misorientations between the constituent cells, as indicated by a very small smearing of the spots of what is essentially a single crystal diffraction pattern. In progressing towards the chip, the microstructure undergoes a drastic change in terms of the proliferation of highly misorientated boundaries between the subgrains. This is indicated by a dramatic change in the diffraction pattern over a very small region, from what was essentially a set of smeared spots around a central bright spot to a pattern consisting of nearly uniform rings around the central spot (Fig. 6(c)) (thus, suggesting a random distribution of the subgrains and large associated misorientation angles between the subgrains). While it would be incorrect to draw quantitative conclusions from the diffraction pattern alone, there is some evidence to suggest that such a transition in the nature of the diffraction pattern is usually accompanied by the formation of highly misoriented subgrains [2,3]. This observation is corroborated by direct measurements of the strain field in 2-D machining using visioplasticity techniques applied to high-speed image sequences of the deformation zone recorded during chip forma-

tion. While these measurements indicate that the strain field is not confined to a narrow region as idealized in the shear plane theory, the greatest increment in the shear strain as the bulk material deforms into a chip is still seen to occur over a very narrow region. This region, which appears to be resemble the classical shear plane, is characterized by large strain increments and strain gradients [10].

4. Conclusions

The microstructure resulting from large strain deformation of peak-aged Al-6061T6 by plane strain chip formation is made up primarily of sub-100 nm grains. There appears to be a weak but statistically significant effect of the magnitude of shear strain on the hardness of the chips even at these very large magnitudes of strain wherein flow stress saturation could typically be expected. TEM study of the evolution of the microstructure across the deformation zone indicates a progressive refinement of the microstructure over a region tens of micrometers thick. An abrupt change in the characteristics of the microstructure occurs over a very small region, as inferred from a rapid change in the properties of the diffraction pattern. We tentatively propose, in light of earlier research relating the qualitative properties of the diffraction pattern to the nature of misorientations, that there exits a small region over which there is a sudden proliferation of high angle boundaries in the microstructure of the material as it is deformed into the chip.

Acknowledgements

We would like to thank the Ford Motor Company, Department of Energy grant 4000031768 (via UT-Batelle), Oak Ridge National Laboratory (ORNL) and the State of Indiana's 21st Century Research and Technology Fund for support of this work. Additional thanks are also due to Drs. Andrew Sherman (Ford) and Ray Johnson (ORNL) for their encouragement of the studies.

References

[1] S. Ferrasse, V.M. Segal, K.T. Hartwig, R.E. Goforth, J. Mater. Res. 12 (1997) 1253–1261.
[2] J.Y. Chang, A. Shan, Mater. Sci. Eng. A 347 (2003) 165–170.
[3] J.Y. Chang, J.S. Yoon, G.H. Kim, Scripta Mater. 45 (2001) 347–354.
[4] W.J. Kim, C.S. Chung, D.S. Ma, S.I. Hong, H.K. Kim, Scripta Mater. 49 (2003) 333–338.
[5] W.J. Kim, J.K. Kim, T.Y. Park, S.I. Hong, D.I. Kim, Y.S. Kim, J.D. Lee, Metall. Mater. Trans. A 33 (2002) 3155–3164.
[6] Z. Horita, T. Fujinami, M. Nemoto, T.G. Langdon, Metall. Mater. Trans. A 31 (2000) 691–701.
[7] P.J. Apps, J.R. Bowen, P.B. Prangnell, Acta Mater. 51 (2003) 2811–2822.
[8] M. C. Shaw, Metal cutting principles, Oxford series on advanced manufacturing, Clarendon, Oxford, 1984.
[9] N. Hansen, X. Huang, D.A. Hughes, Mater. Sci. Eng. A 317 (2001) 3–11.
[10] S. Lee, J. Hwang, M. Ravi Shankar, S. Chandrasekar, W.D. Compton (Eds.), in: Proceedings of the American Society of Mechanical Engineers (ASME) International Mechanical Engineering and Exposition, Anaheim, American Society of Mechanical Engineers, New York, NY, USA, 2004.